JOURNAL OF CATALYSIS 85, 53–62 (1984)

# Catalytic Functionalities of Supported Sulfides

## II. Effect of Support on Mo Dispersion

F. E. MASSOTH, G. MURALIDHAR,[1] AND JOSEPH SHABTAI

*Department of Fuels Engineering, University of Utah, Salt Lake City, Utah 84112*

Received December 29, 1982; revised August 1, 1983

Several Mo and CoMo catalysts on different supports, previously evaluated for thiophene hydrodesulfurization (HDS) and 1-hexene hydrogenation (HYD) activities, were characterized for Mo dispersion in the catalysts. Techniques employed for characterization included XRD, ESCA, and $O_2$ chemisorption of catalysts, and determination of "active OH" on supports. For the calcined (oxide) form of Mo and CoMo catalysts on $Al_2O_3$, several $SiO_2$–$Al_2O_3$ compositions, and $SiO_2$, it was found that essentially monolayer dispersion of the Mo was present on $Al_2O_3$ and low $SiO_2$-containing supports, whereas in the case of high $SiO_2$-containing and $SiO_2$ supports evidence was found for three-dimensional crystallites for the Mo phase. The sulfided form of these catalysts gave essentially the same results. These findings are interpreted in terms of the degree of interaction of the Mo phase with the support. To account for changes in HDS and HYD activities of the catalysts, it is proposed that HDS occurs at vacancies on corner sites and HYD at vacancies on edge sites of the $MoS_2$ phase present.

## INTRODUCTION

In the preceding paper (*1*), we reported on the effects of different supports and additives on three catalytic functionalities of the sulfided CoMo catalyst system, viz., hydrodesulfurization (HDS), hydrogenation (HYD), and hydrocracking. In the present study, we have characterized some of these catalysts by XRD, ESCA, and other techniques in an attempt to understand how the functionalities of the different catalysts vary with changes in catalyst structure resulting from variation in the nature of the support. In particular, we have concentrated on the variation of the HDS and HYD functionalities of Mo and CoMo catalysts on a series of supports consisting of $Al_2O_3$, $SiO_2$–$Al_2O_3$ with different $SiO_2$/$Al_2O_3$ ratios, $SiO_2$, and others.

## EXPERIMENTAL

*Catalysts.* All supports used were obtained from commercial sources. The amount of OH replaceable by fluoride was determined by the method of Yamagata *et al.* (*2*). Catalysts containing 8% Mo or 3% Co 8% Mo on various supports were prepared by incipient wetness impregnation and calcined at 540°C. Catalytic activities at atmospheric pressure were determined sequentially for thiophene hydrodesulfurization (HDS) and 1-hexene hydrogenation (HYD), after presulfiding in 10% $H_2S/H_2$ at 400°C and subsequent exposure to thiophene/$H_2$ at 350 or 400°C overnight. The Mo catalysts were tested at 400°C and the CoMo catalysts at 350°C. Experimental details and activity results are given elsewhere (*1*).

*Characterization methods.* The calcined (oxide) catalysts were characterized by XRD and ESCA. X-Ray analysis was performed on powdered samples using Cu$K\alpha$ radiation. ESCA measurements were made on a Hewlett–Packard 5950B spectrometer using monochromatic Al$K\alpha$ radiation (1486 eV), charge compensation being effected by an electron floodgun. Ground samples were dusted onto double-stick tape. The number of scans was limited in order to reduce error due to charging effects. Spectra of C 1*s*,

[1] Research Associate, 1980–1982.



0021-9517/84 $3.00

Al 2*s*, Si, 2*s*, Mo $3d_{5/2}$, Mo $3d_{3/2}$, Co 2*p*, Mg 2*s*, and Ti 2*p* were recorded. Integrated peak areas, including satellite peaks, were obtained. Binding energies referenced to C 1*s* (285.0 eV) were Mo $3d_{5/2}$, 232.7 eV; Mo $3d_{3/2}$, 235.8; and Co $2p_{3/2}$, 781.1. These values are in good agreement with the literature (*3–5*).

To perform *in situ* measurements on sulfided catalysts, a stainless-steel glove box was attached to the sample arm of the ESCA instrument. The box was purged with purified $N_2$ until tests according to the manufacturer's specifications showed $O_2$ and moisture levels were less than 1–5 ppm. The catalyst was sulfided under flow conditions (10% $H_2S/H_2$, 400°C, 2 h) using a separate reaction system, and, after purging with He for 2 h, was cooled to room temperature. The reactor was sealed off, transferred to the glove box, and the sample removed and placed on the ESCA probe.

Theoretical intensities of Mo to support components were calculated according to the method outlined by Kerhof and Moulijn (*6*). Calculations are based on a model of the catalyst consisting of sheets of support with the active phase located on surfaces between the sheets. Defosse (*7*) has recently demonstrated the validity of the sheet model for $\gamma$-$Al_2O_3$ and Kerhof and Moulijn have applied it to silica catalysts. It is assumed that a similar model applies to the other supports used here. The theoretical intensity ratio for a monolayer of Mo on a support is given by

$$\left(\frac{I_{Mo}}{I_s}\right)_{mono} = \left(\frac{X_{Mo}}{X_s}\right)\left(\frac{\sigma_{Mo}}{\sigma_s}\right) Z, \qquad (1)$$

where subscript *s* stands for support component (Al, Si, or Mg), and *I* is peak integral area, *X* is atomic fraction, $\sigma$ is photoelectron cross-section, and *Z* is a correction factor. The correction term is given by

$$Z = \frac{\beta(1 + e^{-\beta})}{2(1 - e^{-\beta})}, \qquad (2)$$

where $\beta = t/\lambda_s$ and $t = 2/\rho_s S$. Here, $\beta$ is a dimensionless support thickness, *t* is the sheet thickness of the support, $\lambda$ is the escape depth, $\rho_s$ is the average density, and *S* is the surface area of the support. Parameter values used for these calculations are given in Table 1. We have made the additional assumption that these equations can be applied to the separate components of binary oxide supports.

## RESULTS

Properties of the supports are given in Table 2. Except for $TiO_2$, all had sufficient surface area to permit monolayer dispersion of Mo. For the $SiO_2$–$Al_2O_3$ series, the concentration of OH replaceable by F ("active OH") per unit surface area decreased with increase in $SiO_2$ content.

The ratio of ESCA peak intensities of Al to Si for Mo and CoMo oxide catalysts of the $SiO_2$–$Al_2O_3$ support series as a function of support composition are shown in Fig. 1. The straight line in the figure is the calculated slope based on photoelectron cross-sections, viz., $I_{Al}/I_{Si} = 0.76$. The agreement with the experimental data is good and shows that the "surface" composition of the support is not essentially different from its bulk composition.

XRD examination of the supported Mo oxide catalysts showed evidence of crystalline $MoO_3$ for the high $SiO_2$ content and the

TABLE 1

Parameter Values Used in ESCA Calculations

| Component | $\sigma$[a] | $\lambda$ (mn) |
|---|---|---|
| Al 2*s* | 0.75 | 1.3[b] |
| Si 2*s* | 0.99 | 2.0[c] |
| Mo 3*d* | 9.50 | |
| Co 2*p* | 12.62 | |
| Mg 2*s* | 0.57 | |
| Ti 2*p* | 5.22 | |

[a] Ref. (*25*).
[b] Ref. (*26*).
[c] Ref. (*6*).

TABLE 2

Properties of Supports and Supported Catalysts

| Support | | | Mo/support[a] | | | CoMo/Support[b] | | |
|---|---|---|---|---|---|---|---|---|
| Composition | Surf. area ($m^2/g$) | OH concd ($nmol/m^2 \times 10^3$) | XRD[c] | FWHM[d] (eV) | $O_2$[e] chem. (mg/g) | XRD[c] | FWHM[d] (eV) | $O_2$[e] chem. (mg/g) |
| $Al_2O_3$ | 209 | 9.09 | n.f. | 2.4 | 0.58 | n.f. | 2.4 | 0.76 |
| 10% $SiO_2$–$Al_2O_3$ | 331 | 6.98 | n.f. | 2.2 | 0.48 | n.f. | 2.4 | 0.70 |
| 25% $SiO_2$–$Al_2O_3$ | 416 | 6.13 | n.f. | 2.2 | 0.36 | n.f. | 2.1 | 0.59 |
| 75% $SiO_2$–$Al_2O_3$ | 425 | 4.38 | $MoO_3$(?) | 1.8 | 0.19 | $CoMoO_4$(w) | 2.1 | 0.36 |
| $SiO_2$ | 300 | 1.27 | $MoO_3$(s) | 1.9 | 0.05 | $CoMoO_4$(s) | 1.8 | 0.11 |
| 73% $SiO_2$–MgO | 315 | — | $MoO_3$(w) | 2.1 | — | $CoMoO_4$(w) | 2.3 | 0.47 |
| $TiO_2$ | 55 | — | $MoO_3$(m) | 1.6 | — | $CoMoO_4$(m) | 1.4 | 0.13 |

[a] 8% Mo.
[b] 3% Co, 8% Mo.
[c] n.f., no phase found; s, strong; m, moderate; w, weak.
[d] Full width at half maximum for ESCA $Mo_{3d}$ peak.
[e] $O_2$ chemisorption from Ref. (*27*).

$TiO_2$-supported catalysts (Table 2). At least part of the Mo is not highly dispersed in these catalysts. This is further evidenced by narrow Mo ESCA peaks (FWHM values) for these catalysts. In the high $Al_2O_3$ content catalysts, the broader ESCA peaks and the absence of crystalline $MoO_3$ by XRD indicate a high extent of Mo dispersion.

Theoretical values of Mo to support component ESCA intensities for monolayer dispersion are compared to experimental values in Table 3. Reasonably good agreement, indicating essentially monolayer coverage, is obtained for $Al_2O_3$ and 10% $SiO_2$–$Al_2O_3$ catalysts; fair agreement is found for the 25% $SiO_2$–$Al_2O_3$ catalyst. The 75% $SiO_2$–$Al_2O_3$ catalyst also seems to exhibit high Mo dispersion. However, lower dispersions are evident for the 73% $SiO_2$–MgO and particularly the $SiO_2$ catalysts, i.e., less "surface" Mo is detected, in accord with three-dimensional crystallites of $MoO_3$ found in these samples by XRD.

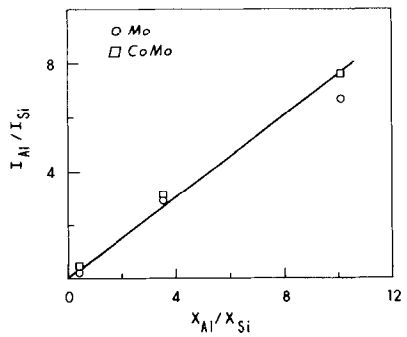


FIG. 1. Variation of Al/Si ESCA intensities with support composition.

As shown in Table 2, the properties of the CoMo catalysts were similar to those of the Mo catalysts with respect to XRD analysis (except that $CoMoO_4$ was observed in place of $MoO_3$) and Mo ESCA peak widths. Calculated vs. experimental $I_{Mo}/I_{Al}$ intensity ratios are given in Table 4. As seen, the trends are generally similar to those of the Mo catalysts for the $SiO_2$–$Al_2O_3$ series. The $I_{Co}/I_{Mo}$ ratios for the $SiO_2$–$Al_2O_3$ series are shown in Fig. 2. The theoretical value is given by

$$\left(\frac{I_{Co}}{I_{Mo}}\right)^* = \left(\frac{X_{Co}\sigma_{Co}}{X_{Mo}\sigma_{Mo}}\right) = 0.81. \qquad (3)$$

The experimental values are less than the theoretical value and a discontinuity in the ratio appears between the 25 and 75% $SiO_2$–$Al_2O_3$ catalysts.

A similar discontinuity is observed in the $O_2$ chemisorption data for the $SiO_2$–$Al_2O_3$ catalysts series, as shown in Fig. 3, although single lines through the points are possible. A discontinuity is also observed in Fig. 4, where relative HDS activities are

TABLE 3

ESCA Intensity Ratios for Mo Catalysts[a]

| Support | $(I_{Mo}/I_{Al})_{mono}$ | $(I_{Mo}/I_{Al})_{expt}$ | $(I_{Mo}/I_{Si})_{mono}$ | $(I_{Mo}/I_{Si})_{expt}$ | $(I_{Mo}/I_{Mg})_{mono}$ | $(I_{Mo}/I_{Mg})_{expt}$ |
|---|---|---|---|---|---|---|
| $Al_2O_3$ | 0.79 (0.49) | 0.77 (0.42) | | | | |
| 10% $SiO_2$–$Al_2O_3$ | 0.76 | 0.76 | 5.80 | 5.10 | | |
| 25% $SiO_2$–$Al_2O_3$ | 0.89 | 0.74 | 2.30 | 2.20 | | |
| 75% $SiO_2$–$Al_2O_3$ | 2.80 | 3.10 | 0.77 | 0.94 | | |
| $SiO_2$ | | | 0.64 (0.37) | 0.23 (0.20) | | |
| 73% $SiO_2$–MgO | | | 0.84 | 0.67 | 2.50 | 1.40 |

[a] Values are for oxide catalysts using Mo $3p_{3/2}$ and Mo $3p_{5/2}$ peaks; values in parentheses are for sulfided catalysts using Mo $3p_{3/2}$ peak.

plotted against "active OH" concentration of the support for the same series of catalysts.

## DISCUSSION

### *1. Dispersion of the Mo Phase*

For the Mo/$SiO_2$–$Al_2O_3$ series, the results indicate a high degree of dispersion of Mo on catalysts containing a high proportion of $Al_2O_3$. On the other hand, the ESCA results show a low Mo dispersion for the $SiO_2$-supported catalyst, in agreement with the presence of three-dimensional $MoO_3$ crystallites as observed by XRD. The ESCA results for the 75% $SiO_2$–$Al_2O_3$ catalyst appear to be anomalous, indicating high dispersion of the Mo whereas other data point to three-dimensional crystallites, e.g., XRD and FWHM (Table 2), $O_2$ chemisorption (Fig. 3) and catalyst activities (Fig. 4). Possible reasons for the discrepancy could be that in this case the theory does not rigorously apply to the separate components of the binary oxide support, and/or that the support may not entirely consist of parallel sheets as assumed in the model.

The ESCA results for the CoMo catalysts are similar to those for the nonpromoted Mo systems. A reasonably high dispersion of the Mo for $Al_2O_3$-rich catalysts is indicated. The somewhat lower $I_{Mo}/I_s$ ratios compared with the Mo catalysts may be due to a Co overlayer on the dispersed Mo phase, as Co was added after Mo in the preparation of the catalysts (*1*). Gajardo *et al.* (*8*) and Okamoto *et al.* (*5*) have reported similar results from ESCA studies. The lower $(I_{Mo}/I_{Al})$ experimental versus monolayer ratio for the 75% $SiO_2$–$Al_2O_3$ catalyst indicates poor Mo dispersion for this catalyst, in line with the presence of $CoMoO_4$ as indicated by XRD; however, the $(I_{Mo}/I_{Si})_{mono}$ for this catalyst (as well as for the

TABLE 4

ESCA Intensity Ratios for CoMo Catalysts[a]

| Support | $(I_{Mo}/I_{Al})_{mono}$ | $(I_{Mo}/I_{Al})_{expt}$ | $(I_{Mo}/I_{Si})_{mono}$ | $(I_{Mo}/I_{Si})_{expt}$ | $(I_{Mo}/I_{Mg})_{mono}$ | $(I_{Mo}/I_{Mg})_{expt}$ |
|---|---|---|---|---|---|---|
| $Al_2O_3$ | 0.82 (0.51) | 0.70 (0.37) | | | | |
| 10% $SiO_2$–$Al_2O_3$ | 0.80 | 0.61 | 6.00 | 4.60 | | |
| 25% $SiO_2$–$Al_2O_3$ | 0.93 | 0.76 | 2.40 | 2.40 | | |
| 75% $SiO_2$–$Al_2O_3$ | 2.90 | 1.90 | 0.81 | 0.95 | | |
| $SiO_2$ | | | 0.66 | 0.22 | | |
| 73% $SiO_2$–MgO | | | 0.87 | 0.96 | 2.70 | 1.90 |

[a] See footnote in Table 3.

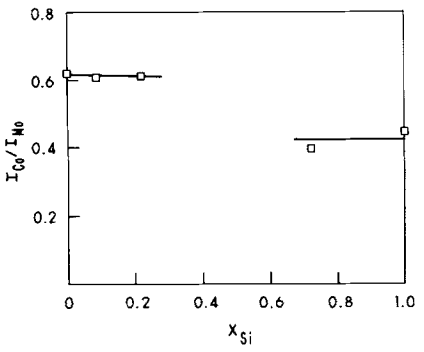


FIG. 2. Variation of Co/Mo ESCA intensities with support composition.

73% $SiO_2$–MgO catalyst) is still anomalously low as before. The $(I_{Co}/I_{Mo})_{expt}$ value for this catalyst is more in line with that of the $SiO_2$ catalyst (Fig. 2).

The experimental values of $I_{Co}/I_{Mo}$ are lower than the theoretical value of 0.81. For the $Al_2O_3$-rich catalysts, this is most likely due to incorporation of some Co in the $Al_2O_3$ phase (*9*), lowering its "surface" concentration relative to that of Mo. Chung and Massoth (*10*) and Wivel *et al.* (*11*) have reported fractions of Co associated with the $Al_2O_3$ of between 10 and 15% for a CoMo/$Al_2O_3$ catalyst of the same composition as used in the present study. This is in reasonably good agreement with the lowering in $I_{Mo}/I_{Co}$ ratios observed, assuming the Co in $Al_2O_3$ is not detected by ESCA. The even lower ratio for the $SiO_2$ catalyst may be explained on the basis of two phases being present, viz., a bulk CoMo phase (observed by XRD) and a more dispersed $MoO_3$ phase. If all the Co is in the form of $CoMoO_4$, some 40% of the Mo should be as $MoO_3$. The latter, not being detected by XRD, must be as small crystallites of an amorphous phase. There would be more contribution to the Mo signal from this phase than from Mo in the $CoMoO_4$ phase, resulting in a lower $I_{Co}/I_{Mo}$ ratio.

### 2. *Active Sites*

Previous studies (*1*) on the same $SiO_2$–$Al_2O_3$-supported catalysts have shown appreciably lower catalytic activities for thiophene HDS and 1-hexene HYD when compared to the $Al_2O_3$-supported catalyst. In particular, for the $SiO_2$–$Al_2O_3$ series the HDS activity dropped sharply and the HYD activity more slowly with increase in $SiO_2$ content, indicating a decrease in active sites for these reactions. Chemisorption of $O_2$ showed a similar trend (Fig. 3). Nevertheless, the present ESCA results show essentially monolayer dispersion of the Mo for the lower $SiO_2$ content catalysts of this series. The basic question then is how can the number of active sites decrease while the Mo remains as a monolayer? We propose to resolve this question in terms of a monolayer cluster model.

It is well known that Mo interacts strongly with $Al_2O_3$ in the oxidic catalyst

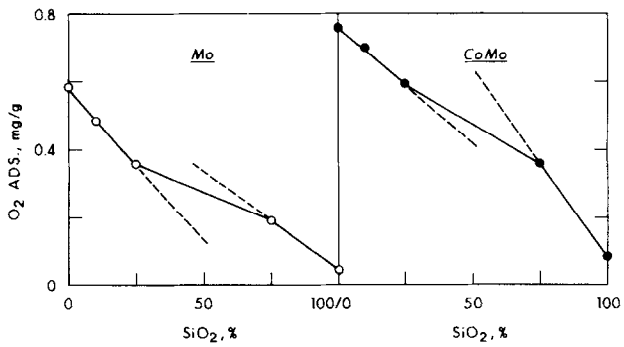


FIG. 3. Variation of $O_2$ chemisorption with change in $SiO_2$ content of $SiO_2$–$Al_2O_3$-supported Mo and CoMo catalysts (*27*).

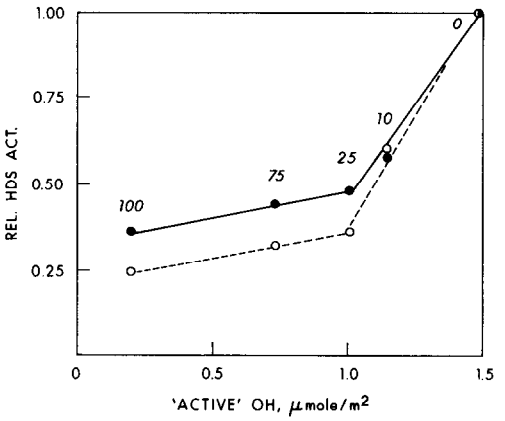


FIG. 4. Relative HDS activities vs $SiO_2$–$Al_2O_3$ "active OH" concentration for Mo (○) and CoMo (●) catalysts. Numbers are percentage $SiO_2$ content.

(*9*). Yamagata *et al.* (*2*) have suggested that the amount of strongly adsorbed Mo depends on the OH content replaceable by F ions on the support. Recent EXAFS studies have shown that Mo oxide on $Al_2O_3$ exists as small, disordered clusters (*12*). *We propose that the Mo cluster depends on the surface concentration of the OH groups,* which in turn is related to the $Al_2O_3$ content. As $SiO_2$ is added to $Al_2O_3$, the OH concentration decreases (Table 2), resulting in less bonding of the Mo to the surface. The clusters thus will grow laterally forming larger clusters, in contrast to $Al_2O_3$ where the clusters are strongly bonded and remain small. As the $SiO_2$ content continues to increase, insufficient bonding sites remain and three-dimensional growth of $MoO_3$ occurs. Only at this state would the Mo dispersion as determined by ESCA decrease, since ESCA cannot distinguish between cluster sizes in a monolayer.

During sulfiding, the Mo oxide phase is converted to a sulfide phase. Several investigations (*13, 14*) have reported that the Mo dispersion does not change during sulfiding, and our ESCA results on the sulfided catalysts are in essential agreement. Furthermore, it has been reported that the cluster size is maintained in the $Mo/Al_2O_3$ catalyst, forming a monolayer of $MoS_2$ (*12*). Accepting then that the Mo dispersion in the sulfided catalyst is roughly the same as in the oxide catalyst, we further propose that *the active sites for HYD occur at edge sites and for HDS at corner sites of the $MoS_2$ structure.*

Stevens and Edmonds (*15*) have suggested that basal (top) plane sites of $MoS_2$ are active for HDS. We cannot reconcile our results with this proposal since the ESCA data showed no essential difference in Mo dispersion for $Al_2O_3$, 10% $SiO_2$–$Al_2O_3$, and 25% $SiO_2$–$Al_2O_3$ catalysts. This indicates no change in the concentration of top layer atoms exposed for these catalysts and consequently no change in catalytic activity would be expected; however, it was found that HDS and HYD activity markedly decreased with increasing $SiO_2$ content.

Termination edges of small $MoS_2$ clusters or crystallites must contain anionic vacancies, i.e., coordinate unsaturated sites. It is believed that these vacancies are the centers for adsorption and reaction of reactants involved in HDS and HYD (*16, 17*). Examination of the $MoS_2$ structure reveals that corner sites have a higher degree of uncoordination than edge sites. It has been observed that pyridine deactivates thiophene HDS significantly more than olefin HYD (*16*). Also, it has been reported that $H_2S$ strongly inhibits HDS but only weakly inhibits HYD (*16*). Furthermore, TPD/TPR studies of adsorbed $H_2S$ on sulfided $Mo/Al_2O_3$ showed evidence of two adsorption sites, a weaker site for associative adsorption and a stronger one for dissociative adsorption of $H_2S$ (*18*); the former could be associated with edge sites and the latter with corner sites. Therefore, it is reasonable to suppose that corner sites, which could have a greater tendency to adsorb pyridine and $H_2S$, are the sites active for HDS. The geometry and coordination of corner and edge sites could be sufficiently different to favor different types of reactions. For example, an anionic vacancy at a corner site exposes a single Mo ion possessing strongly augmented Lewis acidity.

Such a vacancy would be particularly effective in embedding the heteroatom of a thiophene molecule with attendant strong C–S bond polarization needed for subsequent hydrogenolytic cleavage. On the other hand, an anionic vacancy at an edge site exposes two adjacent Mo ions in a configuration particularly favorable for two-point activated adsorption of the double bond of an olefin (*19*).

If it is assumed that HDS takes place at corner sites and HYD at edge sites, and vacancies are proportional to the concentration of these sites, then, qualitatively, relative HDS activity will decrease faster than relative HYD activity as cluster size increases. This is in line with experimental results for the $SiO_2$–$Al_2O_3$ series of catalysts (*1*). Furthermore, if $O_2$ is chemisorbed at vacancies, its adsorption will decrease with increasing cluster size, in agreement with the experimental data (Table 2). Consider a dimensionless cluster size relative to that of the $Mo/Al_2O_3$ catalyst. As cluster size increases (with addition of $SiO_2$), and assuming a square configuration (other geometries give similar results), it can be shown (see Appendix) that

$$N = 1/W^2, \tag{4}$$

where $N$ is the number of clusters of dimensionless width $W$ relative to the $Mo/Al_2O_3$ catalyst. Now the number of edge, $E$, and corner, $C$, sites relative to the $Mo/Al_2O_3$ catalyst is given by

$$E = 1/W \tag{5}$$

$$C = 1/W^2. \tag{6}$$

If a dual site, $D$, consisting of two adjacent sites is required for HDS, then its concentration will be proportional to $C^2$, or

$$D = 1/W^4. \tag{7}$$

These relationships apply to three-dimensional crystallites as well as monolayer clusters (see Appendix). Although we have identified edge and corner sites with an idealized geometric model, actually they need not be located exclusively at these geometric positions, e.g., if clusters are "ragged", some corner-type positions may be located in edges; it would only be required that the ratio of corner/edge sites remains invariant with cluster size for the above relationships to hold.

Figure 5 shows calculated curves for the decrease in the relative concentration of these sites with increase in relative cluster size, $W$. Superimposed on these curves are relative (to the $Mo/Al_2O_3$ catalyst) activity data points for HYD and HDS as determined experimentally for the various Mo catalysts (*1*). The relative HYD activities are placed on the E curve, and the relative HDS values are located at the same $W$ value, that is, the relative HYD value for a given catalyst is fixed on the E curve (hydrogenation sites), which fixes the $W$ value (relative size) for the catalyst, and the relative HDS value is then plotted at the same $W$ value. For the $SiO_2$–$Al_2O_3$ series (open points), increasing $SiO_2$ content corresponds to increasing $W$. The HDS activities of the low $SiO_2$ content catalysts, which showed monolayer dispersion of the Mo, fall on the D curve, implying a dual-vacancy center is involved in HDS on clusters. Kinetic studies of HDS over CoMo/$Al_2O_3$ (where the Mo dispersion is essentially a monolayer (*12*)), have indi-

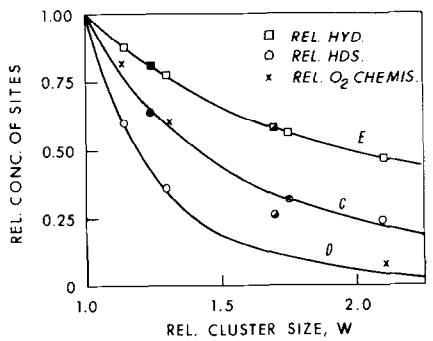


FIG. 5. Change in relative concentration of types of sites as a function of relative cluster size. E—edge sites, C—corner sites, D—dual corner sites; open symbols: $SiO_2$–$Al_2O_3$ series, closed: $TiO_2$, half-closed: $SiO_2$–MgO.

cated a possible dual-vacancy site (*16*). On the other hand, HDS activities for those catalysts exhibiting evidence of three-dimensional crystallites closely follow the C curve, implying only a single vacancy is involved in HDS on $MoS_2$ crystallites. Clusters are probably less well organized then crystallites and would be expected to have more dual-vacancy sites, which may be more favorable for HDS than single sites. Thus, this analysis shows that different site configurations might be involved in HDS reactions, depending on the geometrical form of the $MoS_2$ phase.

We recognize that the assignments regarding the location of HYD and HDS sites are controvertial. In particular, our hypothesis of corner sites active for HDS lacks direct evidence at present; indeed, definitive evidence would be difficult to acquire. One may draw an analogy with reactions over platinum surfaces, where kink sites have been found to be active for C–C bond hydrogenolysis (as well as C–H bond reactions), while step sites are only active for C–H bond reactions (*20*). Corner sites and edge sites on $MoS_2$ can be considered equivalent to kink sites and step sites, respectively on Pt.

It was not possible to develop a similar correlation for the CoMo catalysts because of the added complications of the Co promotion. First, only a fraction of the Co present is active for promoting the HDS activity (*11, 21, 22*). The active fraction has recently been shown to be associated with the Mo sulfide phase in a so-called "Co–Mo–S" structure (*11, 23*), and can vary with the support (*24*). Thus, without direct measurement of this active Co (obtained by Mössbauer emission experiments (*23*)), it was not possible to separate the Co promotional effect from the Mo dispersion effect. Second, Co promotes HDS and hydrogenation reactions to a different extent (*16, 21*). Hence, the promotional selectivity of the active Co on the two reactions would need to be known for each catalyst to develop a meaningful correlation with Mo dispersion. An example of the complicating effect of Co is illustrated by the data given in Table 5, in which $Zn(NO_3)_2$ was added to the $Al_2O_3$ support in one case, and to the $CoMo/Al_2O_3$ catalyst in the second case. The ESCA results indicate a monolayer Mo dispersion in both cases. For the $CoMo/ZnO–Al_2O_3$ catalyst (A), the lower HDS activity (compared to $CoMo/Al_2O_3$) can be partly attributed to a larger cluster size (as for the Mo catalysts discussed above), as evidenced by lower $O_2$ chemisorption. The even greater demise in HDS activity for the other catalyst (B) is most likely due to less effective Co promotion in line with the low $I_{Co}/I_{Mo}$ ratio and identical $O_2$ chemisorption found for this catalyst. The smaller effect

TABLE 5

Effect of ZnO Added by Two Different Methods

| Catalyst | $(I_{Mo}/I_{Al})_{mono}$ | $(I_{Mo}/I_{Al})_{expt}$ | $(I_{Co}/I_{Mo})_{expt}$ | Rel. HYD[a] | Rel. HDS[a] | $O_2$[b] chem. (mg/g) |
|---|---|---|---|---|---|---|
| $CoMo/Al_2O_3$ | 0.83 | 0.70 | 0.62 | 1.00 | 1.00 | 0.76 |
| $CoMo/ZnO–Al_2O_3$ (A)[c] | 0.88 | 0.70 | 0.49 | 0.96 | 0.43 | 0.64 |
| $ZnO + CoMo/Al_2O_3$ (B)[d] | 0.83 | 0.80 | 0.14 | 0.85 | 0.19 | 0.63 |

[a] HYD and HDS activities relative to those of the standard $CoMo/Al_2O_3$ catalyst (Ref. (*1*)).
[b] Ref. (*27*).
[c] 5% of Zn (as $Zn(NO_3)_2$) added to the support prior to CoMo impregnation (Ref. (*1*)).
[d] 5% of Zn (as $Zn(NO_3)_2$) added to the finished $CoMo/Al_2O_3$ catalyst (Ref. (*1*)).

on HYD in this case is evidently due to the fact that Co promotes HYD much less than HDS.

## APPENDIX

Assume a square monolayer cluster of $MoS_2$ of width $w$ and depth $d$. Lateral growth (two-dimensional) increases $w$ at constant $d$ and perpendicular growth (three-dimensional) increases $d$ at constant $w$.

The total volume of $MoS_2$, $V$, is given by

$$V = nmw^2d, \qquad \text{(A-1)}$$

where $n$ is the number of particles and $m$ the number of clusters in a stack (crystallite). Since a cluster consists of two layers of $S$ atoms, the total number of edge $S$ sites, E, and corner sites, C, are

$$S_E = 8nmw \qquad \text{(A-2)}$$

$$S_C = 8nm. \qquad \text{(A-3)}$$

To compare relative particle sizes to that of $Mo/Al_2O_3$, assume the latter is present as monolayer ($m = 1$) clusters of width $w_0$. For a constant amount of Mo,

$$nmw^2d = n_0w_0^2d. \qquad \text{(A-4)}$$

We now define $N = n/n_0$ and $W = w/w_0$ where $N$ is the relative number of particles and $W$ the relative particle width compared to the $Mo/Al_2O_3$ catalyst. Equation (A-4) now becomes

$$NmW^2 = 1. \qquad \text{(A-5)}$$

The relative number of edge sites compared to $Mo/Al_2O_3$ is then

$$E = \frac{8nmw}{8n_0w_0} = NmW = \frac{1}{W} \qquad \text{(A-6)}$$

and similarly for relative corner sites,

$$C = \frac{8nm}{8n_0} = Nm = \frac{1}{W^2}. \qquad \text{(A-7)}$$

For relative dual corner sites, their concentration will be proportional to the square of the relative concentration of corner sites, viz.,

$$D = C^2 = \frac{1}{W^4}. \qquad \text{(A-8)}$$

Thus, the relative site concentrations as a function of cluster or particle width are the same whether growth is lateral, perpendicular, or a combination of these, provided all the clusters in a three-dimension stack have the same cluster width.

## ACKNOWLEDGMENTS

We thank Dr. W. Zmierczak for the OH determinations. The support of the U.S. Department of Energy and the State of Utah is gratefully acknowledged.

## REFERENCES

1. Muralidhar, G., Massoth, F. E., and Shabtai, J., *J. Catal.* **85,** 44 (1984).
2. Yamagata, N., Owada, Y., Okazaki, S., and Tanabe, K., *J. Catal.* **47,** 358 (1977).
3. Lepage, F., Baillif, P., and Bardolle, J., *C.R. Acad. Sci. Paris Ser. C* **280,** 1089 (1975).
4. Patterson, T. A., Carver, J. C., Leyden, D. E., and Hercules, D. M., *J. Phys. Chem.* **80,** 1700 (1976).
5. Okamoto, Y., Imanaka, T., and Teraneski, S., *J. Catal.* **65,** 448 (1980).
6. Kerkhof, F. P. J. M., and Moulijn, J. A., *J. Phys. Chem.* **83,** 1612 (1979).
7. Defosse, C., *J. Electron Spectrosc. Relat. Phenom.* **23,** 157 (1981).
8. Gajardo, P., Grange, P., and Demon, B., *J. Catal.* **63,** 201 (1980).
9. Massoth, F. E., "Advances in Catalysis," Vol. 27, p. 265, Academic Press, New York, 1978.
10. Chung, K. S., and Massoth, F. E., *J. Catal.* **64,** 332 (1980).
11. Wivel, R., Candia, R., Clausen, B. S., Mørup, S., and Topsøe, H., *J. Catal.* **68,** 453 (1981).
12. Clausen, B. S., Topsøe, H., Candia, R., Villadsen, J., Lengeler, B., Als-Nielsen, J., and Christensen, F., *J. Phys. Chem.* **85,** 3868 (1981).
13. Topsøe, N., *J. Catal.* **64,** 235 (1980).
14. Grimblot, J., Dufresne, P., Gengembre, L., and Bonnelle, J., *Bull. Soc. Chim. Belg.* **90,** 1261 (1981).
15. Stevens, G. C., and Edmonds, T., *J. Less-Common Met.* **54,** 321 (1977).
16. Massoth, F. E., and Muralidhar, G., "Proceedings, Climax Fourth International Conference on the Chemistry and Uses of Molybdenum (H. F. Barry and P. C. H. Mitchell, Eds.), p. 343. Climax Molybdenum Co., Ann Arbor, Michigan, 1982.
17. Schuit, G. C. A., *Int. J. Quantum Chem. Suppl. 2* **12,** 43 (1977).
18. Ramachandran, R., and Massoth, F. E., *Canad. J. Chem. Eng.* **60,** 17 (1982).

*19.* Bond, G. C., "Catalysis of Metals." Academic Press, New York, 1962.
*20.* Somorjai, G. A., "Advances in Catalysis," Vol. 26, p. 1. Academic Press, New York, 1977.
*21.* Massoth, F. E., and Chung, K. S., "Proceedings, 7th International Congress on Catalysis," p. 629.
*22.* Topsøe, H., Clausen, B. S., Candia, R., Wivel, C., and Mørup, S., *Bull. Soc. Chim. Belg.* **90,** 1189 (1981).
*23.* Topsøe, H., "Surface Properties and Catalysis by Non-Metals: Oxides, Sulfides and other Transition Metal Compound," p. 326. Reidel, Dordrecht, 1983.
*24.* Candia, R., Clausen, B. S., and Topsøe, H., *J. Cat.* **77,** 564 (1982).
*25.* Scofield, J. H., *J. Electron Spectrosc. Relat. Phenom.* **8,** 129 (1976).
*26.* Penn, D. R., *J. Electron Spectrosc. Relt. Phenom.* **9,** 29 (1976).
*27.* Zmierzak, W., Muralidhar, G., and Massoth, F. E., *J. Catal.* **77,** 432 (1982).